Journal of Solid Mechanics Vol. 12, No. 4 (2020) pp. 814-828
DOI: 10.22034/jsm.2019.1878493.1495

Vibration Analysis of Vessels Conveying Blood Flow Embedded in Viscous Fluid

R. Bahaadini [1,*], M. Hosseini [2], M.A. Paparisabet [2]

[1]*Department of Mechanical Engineering, Shahid Bahonar University of Kerman, Kerman, Iran*
[2]*Department of Mechanical Engineering, Sirjan University of Technology, Sirjan, Iran*

Received 17 July 2020; accepted 20 September 2020

ABSTRACT

Vibration analysis of vessels conveying blood flow embedded in viscous fluid is studied based on the modified strain gradient theory. The viscoelastic vessels are simulated as a non-classical Euler-Bernoulli beam theory. Employing Hamilton's principle, the governing equations for size-dependent vessels are derived. The Galerkin method is used in order to transform the resulting equations into general eigenvalue equations. The effects of the blood flow profile and its modification factors, red blood cells (RBCs) and hematocrit are considered in the blood flow. Besides, the influences of the constitutional material gradient scale, blood flow, internal pressure, structural damping coefficient, viscous fluid substrate and various boundary conditions on the natural frequencies and critical buckling velocities are studied. It is revealed that as the hematocrit, fluid viscosity of substrate, internal pressure and mass ratio increase, the natural frequencies and critical buckling velocities decrease. Furthermore, the results indicated that the strain gradient theory predicts the highest natural frequencies and critical buckling velocities among others. The results are compared with those available in the literature and good agreement has been observed.

Keywords: Vessel; Blood; Modified strain gradient theory; Hematocrit; Viscous substrate.

1 INTRODUCTION

THERE is a tremendous growing need of synthetic small diameter grafts that have high long-term patency rate. Vascular community is hardly trying to remove the limitations and obstacles for making synthetic grafts [1]. One of the most usable tools for the future surgeries is the artificial blood vessels. By using artificial blood vessels many of the surgical problems would solved. Therefore, knowing all about the hidden scientific aspects of the blood vessels are essential. If a blood vessel fails or raptures fatal consequences such as strokes or physiological dysfunctions may follow. In this study, the mechanical behavior of the micro blood vessels and the effects of blood flow through it has illuminated. Numerous experimental and theoretical studies have been conducted to predict the behavior of the blood vessels [2-9]. Mechanical stability of the blood vessels and arteries, especially blood vessels

*Corresponding author.
E-mail address: rezabaha67@gmail.com (R. Bahaadini).

buckling, are the most interesting issues to the researchers. There are terms that should be considered in order to predict the stability condition of a blood vessel. Surrounding tissues, blood pressure and vessel's axial tension are some terms that should be calculated in the equations [10]. Han [3] studied the buckling behavior of a blood vessel by considering a soft surrounding tissue support and a static blood pressure. After a while, Liu and Han [11] analyzed the buckling behavior of a blood vessel by the means of pulsatile blood pressure that is more accurate and more real. They have concluded that the maximum buckling pressure in the static state and the pulsatile state approximately have the same values. Khalafvand and Han [12] performed a fluid structure interaction (FSI) study to clarify the buckling and post buckling behavior of the blood vessels. Recently, Hosseini and Paparisabet [13] have shown that the blood flow and suspension particles thorough it have effects on the buckling behavior of the blood vessels. Another factor that has effect on the stability condition and the vibrational behavior is the blood flow. Blood flow has been the subject of numerous studies during the past decades [14-16]. Many try to model the blood flow through the blood vessels. The Refs. [17-19] assumed the blood flow as a single-phase homogeneous Newtonian viscous fluid, a classical approach that did not consider the red blood cells (RBCs). This approach was approximately suitable for the big blood vessels such as aorta but it does not adequate for the small blood vessels (blood vessel's diameter less than 1000 micrometer). By passing time, it has revealed that the RBCs have a vital role in the circulatory system and experimental data has shown that the red blood cells have a substantial part in the blood flow profile especially in the small blood vessels [20]. Therefore, researchers have considered a two-phase fluid for the blood flow [17, 21, 22]. A peripheral layer that consists of plasma and it does not have any other particles and a central region or core that is a mixture of the plasma and suspension particles [3]. These suspension particles are called erythrocytes (small spherical nonflexible particles). It should be mentioned that particles are composed of RBCs, white blood cells and platelets. Given the small size of platelets and less substantially numerous number of white blood cells in comparison with the size and the number of red blood cells respectively, we assume all the suspension particles as RBCs. As it mentioned before, central core region is made of the erythrocytes and plasma. Therefore, the viscosity of the plasma layer and the central core region are different from each other [17]. Blood viscosity depends on the hematocrit, i.e., the volume fraction of suspension particles to total blood volume [17]. Because of the difference between the various phase's viscosity, the blood flow velocity is differs from one phase to another. Blood vessels can be simulated as the pipes conveying fluid. Many researchers have investigated over the macro pipes conveying fluid and the governing equations are extracted [23-27]. Due to the recent technological enhancements micro scale pipes such as: fluid storage, drug delivery and micro-and nano- fluidic devices are more usable and operational. In the last two decades, experimental studies have performed about size-dependent deformation behavior of microstructures; the reader is referred to Refs. [28-31]. They have shown that classical continuum mechanics is not capable of predicting sized-effect on the mechanical behaviors and the sized-effect plays a substantial role in microstructures. Therefore, size-dependent continuum theories such as Eringen's nonlocal elasticity, modified couple stress elasticity and modified strain gradient elasticity theories have been developed [32-34]. The modified strain gradient theory is one of the higher-order continuum theories, which considers the antisymmetric and symmetric parts of the higher order deformation gradients. In this regard, recent developments in the vibrational behavior of interaction between fluid and structure can be pursued in the work of Hosseini and Sadeghi-Goughari [35], Bahaadini et al. [36-45], Bahaadini and Saidi [46-49], Saidi et al. [50], Mohammadi et al. [51], Cabrera-Miranda and Paik [52], Farajpour et al. [53], Amiri et al. [54], Ebrahimi et al. [55], Mohammadimehr and Mehrabi [56], Arani et al. [27, 57, 58], Atashafroz et al. [59], Hosseini et al. [60-62] and Arani and Soleymani [63-65]. Up to now, numerous studies have been implemented to investigate the static mechanical behavior of the blood vessels.

In this study, the modified strain gradient beam model is considered to analyze the vibration of the viscoelastic vessels conveying blood flow and embedded in the viscous fluid. The governing equation of motion and related boundary conditions are obtained via variational Hamilton's principle. Using Galerkin's approximate method, the partial differential equations are converted to ordinary differential equations. In numerical analysis, the effects of internal length scale, viscoelastic structural damping coefficient and other physically parameters such as hematocrit, internal pressure, blood flow profile and the RBCs diameter on the frequencies and critical blood velocities of the blood vessels are investigated. This literature is drawing a better point of view for an uprising issue.

2 MATHEMATICAL MODELING

A schematic configuration of the micro blood vessel conveying blood flow and embedded in viscous fluid is illustrated in Fig.1. The micro vessel has the length L, inner radius R_i , outer radius R_o and radius of mixture phase

R_1 as shown in Fig.1. It is assumed that the mass per unit length of the micro vessel and that of the blood flow has been defined by m_v and m_b, respectively.

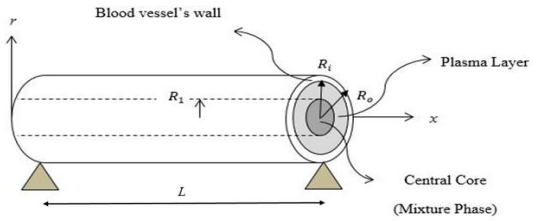

Fig.1
Schematic of the blood-conveying vessel.

2.1 Modified strain gradient theory

According to the modified strain gradient theory, the strain energy density is a function of the higher-order deformation gradients like symmetric strain tensor, dilatation gradient vector, deviatoric stretch gradient tensor and symmetric rotation gradient tensor [34]. Consequently, the stored strain energy E_e in a continuum made of an isotropic linear elastic material occupying region V can be written with infinitesimal deformations as:

$$E_e = \frac{1}{2}\int_V \left(\sigma_{ij}\varepsilon_{ij} + p_i\gamma_i + \tau_{ijk}^{(1)}\eta_{ijk}^{(1)} + m_{ij}\chi_{ij}\right)dV \tag{1}$$

In which, classical stress tensor σ and higher-order stress tensors $\boldsymbol{p}$, $\boldsymbol{\tau^{(1)}}$ and $\boldsymbol{m}$ can be formulated as below [66]:

$$\sigma_{ij} = \lambda\delta_{ij}\varepsilon_{mm} + 2G\varepsilon_{ij} \tag{2a}$$

$$p_i = 2l_0^2 G\gamma_i \tag{2b}$$

$$\tau_{ijk}^{(1)} = 2l_1^2 G\eta_{ijk}^{(1)} \tag{2c}$$

$$m_{ij} = 2l_2^2 G\chi_{ij} \tag{2d}$$

The parameters λ and G denote the bulk and the shear modules in the constitutive equation of the classical stress σ_{ij}, respectively. Also, l_0, l_1 and l_2 stand for three independent material length scale parameters related to dilatation, deviatoric stretch and rotation gradients, respectively. Also, the components of the classical strain tensor $\boldsymbol{\varepsilon}$, the dilatation gradient vector $\boldsymbol{\gamma}$, the deviatoric stretch gradient tensor $\boldsymbol{\eta^{(1)}}$ and the symmetric rotation gradient tensor $\boldsymbol{\chi}$ are represented by ε_{ij}, γ_i, $\eta_{ijk}^{(1)}$ and χ_{ij} respectively and they are defined as following:

$$\varepsilon_{ij} = \frac{1}{2}(u_{i,j} + u_{j,i}) \tag{3a}$$

$$\gamma_i = \varepsilon_{mm,i} \tag{3b}$$

$$\eta_{ijk}^{(1)} = \frac{1}{3}(\varepsilon_{jk,i} + \varepsilon_{ki,j} + \varepsilon_{ij,k}) - \frac{1}{15}\delta_{ij}(\varepsilon_{mm,k} + 2\varepsilon_{mk,m}) - \frac{1}{15}[\delta_{jk}(\varepsilon_{mm,i} + 2\varepsilon_{mi,m}) + \delta_{ki}(\varepsilon_{mm,j} + 2\varepsilon_{mj,m})] \tag{3c}$$

$$\chi_{ij} = \frac{1}{2}(\theta_{i,j} + \theta_{j,i}) \tag{3d}$$

$$\theta_i = \frac{1}{2}(curl\,(u))_i \tag{3e}$$

Here u_i is the component of displacement vector in x_i direction, θ_i is the infinitesimal rotation vector θ and δ_{ij} is the Kronecker delta function.

The displacements of an arbitrary point along the *x*-, *y*- and *z*-axes based on the Euler-Bernoulli beam theory can be expressed as follow:

$$u = -z\,\frac{\partial w\,(x\,,t\,)}{\partial x}\quad,\ v = 0\,,\quad w = w\,(x\,,t\,) \tag{4}$$

where $w\,(x\,,t\,)$ stands for the lateral deflection. Substituting Eq. (4) into Eq. (3a) the non-zero components of the strain-displacement relations can be expressed as:

$$\varepsilon_{xx} = -z\,\frac{\partial^2 w\,(x\,,t\,)}{\partial x^{\,2}} \tag{5}$$

By inserting Eqs. (4) and (5) into Eqs. (3), the non-zero components of γ_i, $\eta^{(1)}_{ijk}$ and χ_{ij} can be obtained as:

$$\gamma_x = -z\,\frac{\partial^3 w}{\partial x^{\,3}},\quad \gamma_y = 0,\quad \gamma_z = -\frac{\partial^2 w}{\partial x^{\,2}} \tag{6a}$$

$$\begin{aligned}
&\eta^{(1)}_{113} = \eta^{(1)}_{131} = \eta^{(1)}_{311} = -\frac{4}{15}\frac{\partial^2 w}{\partial x^{\,2}},\quad \eta^{(1)}_{122} = \eta^{(1)}_{212} = \eta^{(1)}_{221} = \frac{1}{5}z\,\frac{\partial^3 w}{\partial x^{\,3}},\\
&\eta^{(1)}_{223} = \eta^{(1)}_{232} = \eta^{(1)}_{322} = \frac{1}{15}\frac{\partial^2 w}{\partial x^{\,2}},\quad \eta^{(1)}_{133} = \eta^{(1)}_{313} = \eta^{(1)}_{331} = \frac{1}{5}z\,\frac{\partial^2 w}{\partial x^{\,2}},\\
&\eta^{(1)}_{111} = -\frac{2}{5}z\,\frac{\partial^3 w}{\partial x^{\,3}},\quad \eta^{(1)}_{333} = \frac{1}{5}\frac{\partial^2 w}{\partial x^{\,2}}
\end{aligned} \tag{6b}$$

$$\chi_{xy} = \chi_{yx} = -\frac{1}{2}\frac{\partial^2 w}{\partial x^{\,2}} \tag{6c}$$

Afterward, by substituting Eqs. (5) and (6) into Eqs. (2), the non-zero higher order stress components can be obtained as:

$$p_x = -2l_0^2 Gz\,\frac{\partial^3 w}{\partial x^{\,3}},\qquad p_z = -2l_0^2 Gz\,\frac{\partial^2 w}{\partial x^{\,2}} \tag{7a}$$

$$\begin{aligned}
&\tau^{(1)}_{113} = \tau^{(1)}_{131} = \tau^{(1)}_{311} = -\frac{8}{15}l_1^2 G\,\frac{\partial^2 w}{\partial x^{\,2}},\quad \tau^{(1)}_{122} = \tau^{(1)}_{212} = \tau^{(1)}_{221} = \frac{2}{5}l_1^2 Gz\,\frac{\partial^3 w}{\partial x^{\,3}},\\
&\tau^{(1)}_{223} = \tau^{(1)}_{232} = \tau^{(1)}_{322} = \frac{2}{15}l_1^2 G\,\frac{\partial^2 w}{\partial x^{\,2}},\quad \tau^{(1)}_{133} = \tau^{(1)}_{313} = \tau^{(1)}_{331} = \frac{2}{5}l_1^2 Gz\,\frac{\partial^3 w}{\partial x^{\,3}},\\
&\tau^{(1)}_{111} = -\frac{4}{5}l_1^2 Gz\,\frac{\partial^3 w}{\partial x^{\,3}},\quad \tau^{(1)}_{333} = \frac{2}{5}l_1^2 G\,\frac{\partial^2 w}{\partial x^{\,2}}.
\end{aligned} \tag{7b}$$

$$m_{xy} = m_{yx} = -l_2^2 G\,\frac{\partial^2 w}{\partial x^{\,2}}. \tag{7c}$$

Based on the above-mentioned relations, the strain energy of micro vessel can be expressed as:

$$E_e = \frac{1}{2}\int_0^L \left[S\left(\frac{\partial^2 w}{\partial x^2}\right)^2 + K\left(\frac{\partial^3 w}{\partial x^3}\right)^2 \right] dx . \tag{8a}$$

where

$$K = GI\left(2l_0^2 + \frac{4}{5}l_1^2\right), \quad S = EI + GA(2l_0^2 + \frac{8}{15}l_1^2 + l_2^2). \tag{8b}$$

In which I and A are the respective moment of inertia and the cross-sectional area of the micro vessel. Assuming continuously connected foundation, the effect of the external viscous fluid were studied by Ghavanloo and Fazelzadeh [67]. The surface traction virtual work of the surrounding viscous fluid around the blood vessel, q is given by

$$\delta W_f = -\int_0^L q\,\delta w dx \tag{9a}$$

where

$$q = c_0 \frac{\partial w}{\partial t},\ c_0 = \frac{2\mu_f \pi(\eta^2 - 1)}{1 - \eta^2 + (1+\eta^2)Ln(\eta)}\ ,\ \eta = \frac{R_o}{h_1} \tag{9b}$$

It should be noted that the parameter c_0 is positive ($0<\eta<1$). Here, R_o is micro blood vessel (MBV) outer radius and h_1 is the distance from the centerline to the position where the induced viscous surrounding flow vanished. To couple the elastic deformation of the MBV and the viscous flow of the external fluid, we assume that the surface traction of the external fluid along the interface is equal to external force exerted on the MBV.

Moreover, the work done by the internal pressure p can be obtained:

$$W_p = \frac{1}{2}\int_0^L p\pi R_i^2 (\frac{\partial w}{\partial x})^2 dx \tag{10}$$

The first vibrational of kinetic energy of micro vessel and blood are demonstrated in the following

$$\delta T_v = m_v \int_0^L \frac{\partial w}{\partial t}\frac{\partial \delta w}{\partial t} dx \tag{11}$$

$$\delta T_b = m_b \int_0^L \left[\frac{\partial w}{\partial t}\frac{\partial \delta w}{\partial t} + \bar{u}\frac{\partial w}{\partial t}\frac{\partial \delta w}{\partial x} + \bar{u}\frac{\partial w}{\partial x}\frac{\partial \delta w}{\partial t} + \bar{u}^2 \frac{\partial w}{\partial x}\frac{\partial \delta w}{\partial x} \right] dx \tag{12}$$

In which m_b and $\bar{u}$ denote mass per unit length of blood and blood velocity, respectively.

2.2 Modification factors

The non-uniformity of the blood flow distribution is considered by modification factors. Therefore, the Centrifugal force term and the Coriolis term of equation is driven by the assist of mean velocity $\bar{u}$ and blood mass per the unit length m_b as:

$$-\frac{\partial^2 w}{\partial x^2}\int u^2 \rho dA = -\frac{\partial^2 w}{\partial x^2}\int 2\pi r u^2 \rho dr = -\frac{\partial^2 w}{\partial x^2}\alpha_1 m_b \bar{u}^2 \tag{13}$$

$$-\frac{\partial^2 w}{\partial x\,\partial t}\int u\rho dA=-\frac{\partial^2 w}{\partial x\,\partial t}\int 2\pi ru\rho dr=-\frac{\partial^2 w}{\partial x\,\partial t}\alpha_2 m_b\bar{u} \tag{14}$$

$$\alpha_1=\frac{\int 2\pi ru^2\rho dr}{m_b\bar{u}^2} \tag{15}$$

$$\alpha_2=\frac{\int 2\pi ru\rho dr}{m_b\bar{u}} \tag{16}$$

where α_1 and α_2 are modification factors. These modification factors are used into the governing equation in order to calculate the non-uniformity of blood flow distributions.

For finding the modification factors (from Eqs. (15, 16)), four terms should be calculated, namely $\int 2\pi ru^2\rho dr$, $\int 2\pi ru\rho dr$, $\bar{u}$ and m_b, as:

$$\begin{aligned}\int 2\pi ru^2\rho dr&=2\pi\int_{R_1}^{R_i} r\rho_{pl}u^2{}_{plasma}dr+2\pi(1-c)\int_0^{R_1} r\rho_{cc}u^2{}_{central\ fluid}dr+2\pi c\int_0^{R_1} r\rho_{pa}u^2{}_{particle}dr\\ \int 2\pi ru\rho dr&=2\pi\int_{R_1}^{R_i} r\rho_{pl}u_{plasma}dr+2\pi(1-c)\int_0^{R_1} r\rho_{cc}u_{central\ fluid}dr+2\pi c\int_0^{R_1} r\rho_{pa}u_{particle}dr\end{aligned} \tag{17}$$

$$\bar{u}=\frac{2\pi\int_1^{R_i} ru_{plasma}dr+2\pi(1-c)\int_0^{R_1} ru_{central\ fluid}dr+2\pi c\int_0^{R_1} ru_{particle}dr}{A} \tag{18}$$

$$m_b=2\pi\int_{R_1}^{R_i} r\rho_{pl}dr+2\pi(1-c)\int_0^{R_1} r\rho_{cc}dr+2\pi c\int_0^{R_1} r\rho_{pa}dr \tag{19}$$

In which, r and x are radial and axial coordinates respectively, and $u_{central\ fluid}$ and $u_{particle}$ are the axial velocity of blood and particle in core region $(0\le r\le R_1)$, respectively. Also, u_{plasma} is the blood velocity in the peripheral region $(R_1\le r\le R_i)$ and c denotes the hematocrit. The relationship between R_i and R_1 ($R_1=\delta R$) is based on experimental equations [17]. δ is calculated from the relation: $\delta=1-\varepsilon/R_i$, where $\varepsilon\cong\varepsilon(c)$ denotes the peripheral layer thickness for a given hematocrit [68]. Furthermore, A is the total vessel cross section area ($A=\pi R_i^2$); ρ_{pl} is the plasma layer density; ρ_{cc} is the central core region density, and ρ_{pa} is the particle density.

To simplify the analysis, the following dimensionless variables and expressions are defined:

$$\begin{aligned}&W=\frac{w}{L},\quad X=\frac{x}{L},\quad U=\left(\frac{m_{b45\%}}{EI}\right)^{0.5}\bar{u}L,\quad \beta=\frac{m_{b45\%}}{m_{b45\%}+m_v},\quad T=\frac{t}{L^2}\left(\frac{EI}{m_{b45\%}+m_v}\right)^{0.5},\quad \beta_0=\frac{m_b}{m_{b45\%}},\\ &g=\frac{\alpha}{L^2}\left(\frac{EI}{m_b+m_v}\right)^{0.5},\ \mathrm{P}=\frac{p\pi R_i^2L^2}{EI},\ \mathrm{C}=\frac{c_0L^2}{EI\,(m_{b45\%}+m_v)^{0.5}},\ \xi=\frac{8\left(2r_0^2+8r_1^2/15+1\right)}{(1+\upsilon)\left(1+\hbar^2\right)\phi_1^2},\quad \kappa=\frac{r_0^2+2r_1^2/5}{(1+\upsilon)\phi_2},\\ &r_0=\frac{l_0}{l_2},\quad r_1=\frac{l_1}{l_2},\quad \phi_1=\frac{2R_o}{l_2},\quad \phi_2=\frac{L}{l_2},\quad \hbar=\frac{R_i}{R_o}.\end{aligned} \tag{20}$$

In which $m_{b45\%}$ is a blood mass, which has 45% hematocrit. The Hamilton's principle for vessels containing blood flow is given by Benjamin [69]

$$\delta\int_0^t\left(T_v+T_b-E_e+W_f+W_p\right)dx=0 \tag{21}$$

By substituting Eqs. (8)-(12) into Eq. (21) and based on Kelvin-Vogit viscoelastic model with structural damping coefficient α, Young's modulus E and shear modulus G are replaced with the operator $E(1+\alpha\partial/\partial t)$ and $G(1+\alpha\partial/\partial t)$, respectively [67], the non-classical governing equation of motion is derived as:

$$\begin{aligned}&-g\kappa\frac{\partial^7 W}{\partial X^6\partial T}-\kappa\frac{\partial^6 W}{\partial X^6}+g(1+\xi)\frac{\partial^5 W}{\partial X^4\partial T}+(1+\xi)\frac{\partial^4 W}{\partial X^4}+(\alpha_1\beta_0U^2+P)\frac{\partial^2 W}{\partial X^2}\\&+2\alpha_2U\beta_0\beta^{1/2}\frac{\partial^2 W}{\partial X\,\partial T}+C\frac{\partial W}{\partial T}+\left(1+\beta(\beta_0-1)\right)\frac{\partial^2 W}{\partial T^2}=0\end{aligned} \tag{22}$$

In addition, the boundary conditions obtained from Hamilton's principle for micro vessel conveying blood is written as:

For Pinned-Pinned condition at X=0, 1, W=0,

$$-g\kappa\frac{\partial^5 W}{\partial X^4\partial T}-\kappa\frac{\partial^4 W}{\partial X^4}+g(1+\xi)\frac{\partial^3 W}{\partial X^2\partial T}+(1+\xi)\frac{\partial^2 W}{\partial X^2}=0\ ,\ \ \kappa\frac{\partial^3 W}{\partial X^3}=0 \tag{23a}$$

For Clamped-Pinned condition at X=0 , W=0,

$$\frac{\partial W}{\partial X}=0\,,\quad \kappa\frac{\partial^3 W}{\partial X^3}=0\,.$$

at X=1, W=0, (23b)

$$-g\kappa\frac{\partial^5 W}{\partial X^4\partial T}-\kappa\frac{\partial^4 W}{\partial X^4}+g(1+\xi)\frac{\partial^3 W}{\partial X^2\partial T}+(1+\xi)\frac{\partial^2 W}{\partial X^2}=0\,,\quad \kappa\frac{\partial^3 W}{\partial X^3}=0$$

For Clamped-Clamped condition at X=0, 1, W=0,

$$\frac{\partial W}{\partial X}=0\,,\quad \kappa\frac{\partial^3 W}{\partial X^3}=0\,. \tag{23c}$$

3 SOLUTION PROCEDURES

3.1 Galerkin approach

In this section, the extended Galerkin approach is used to solve the governing equation and boundary conditions. In this technique, we must choose weighting functions that are only essential to satisfy boundary conditions. The normalized transverse displacement W is approximated as:

$$W(X,T)=\sum_{r=1}^{n}q_r(T)\phi_r(X) \tag{24}$$

where $q_r(T)$ and n are the generalized coordinates and the number of modes, respectively. Also, $\phi_r(X)$ represents free vibration natural modes of bending which are expressed as [70]:

$$\phi_r(X)C_1\sin\sigma_rX+C_2\cos\sigma_rX+C_3\sinh\sigma_rX+C_4\cosh\sigma_rX \tag{25}$$

where σ_r represents *rth* dimensionless eigenvalue of the *rth* flexural mode $\phi_r(X)$ and C_1,C_2,C_3,C_4 are constant coefficients which are obtained from the boundary conditions. By substituting the displacement field in the

governing equation and using extended Galerkin method, the discretized form of the governing equation of motion for the micro vessel conveying blood flow can be obtain as:

$$[M]\{\ddot{q}(T)\}+[C]\{\dot{q}(T)\}+[K]\{q(T)\}=0 \tag{26}$$

where $\{q(T)\}$ is the vector of generalized coordinates and the dot notation refers to derivative with respect to time. $[M]$, $[C]$ and $[K]$ correspond to the mass, damping and stiffness matrices of micro vessel, respectively, with the following elements:

$$\begin{aligned}
&M(r,s)=\int_0^1(1+\beta(\beta_0-1))\phi_r(X)\phi_s(X)dX\\
&C(r,s)=\int_0^1[-g\kappa\phi_r'''(X)\phi_s'''(X)+g(1+\xi)\phi_r''(X)\phi_s''(X)+2\alpha_1 u\beta_0\sqrt{\beta}u\phi_r'(X)\phi_s(X)\\
&+C\phi_r(X)\phi_s(X)]dX\\
&K(r,s)=\int_0^1[-\kappa\phi_r'''(X)\phi_s'''(X)+(1+\xi)\phi_r''(X)\phi_s''(X)+\alpha_2\beta_0u^2\phi_r''(X)\phi_s(X)\\
&-P\phi_r'(X)\phi_s'(X)]dX
\end{aligned} \tag{27}$$

The Eigen frequencies for this system are found by rewriting Eq. (26) in first order form and solving the associated eigenvalue problem numerically. The stability and instability zones and type of instability can be examined based on the sign and magnitude of the real and imaginary parts of the eigenvalues [71].

4 RESULTS AND DISCUSSION

4.1 Validation of the study

In order to assess the validation of the current study, the numerical results are presented to compare with those available in the literature. The effects of the material length scales, surrounding tissues, axial tensions and blood flow profile are ignored in order to make a comparison. Therefore, Table 1 shows the dimensionless critical buckling velocity for a single phase blood flow that is reported by the current method, Paidoussis [72] and Ni et al. [73]. The results show an acceptable agreement. In another comparative study, the dimensionless critical buckling velocity is computed for the multi-phase blood flow. Table 2 shows a good agreement between this approach and those that reported by Hosseini and Paparisabet [13]. In addition, we can show the blood flow profile non-uniformity modification factor accuracy. When the blood flow assumed as a single phase fluid then the profile modification factor is equal to 1.333 which has the same value with that reported by Guo et al. [74] for the laminar flow in the circular pipes. In the last comparative study, the natural frequency versus the fluid velocity of the simply supported pipe is investigated without considering the influences of the blood flow effects, surrounding tissue and viscoelastic structural. As it can be observed in Fig.2, there is a very good agreement between the current method and those reported by Yin et al. [66].

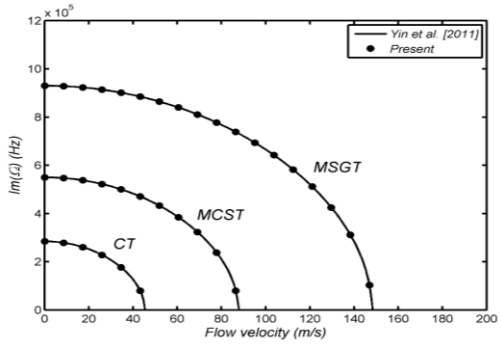

Fig.2
First natural frequency versus the flow velocity for compared with Ref. [66] for *P=0, C=0, g=0,* $\alpha_1=\alpha_2=1$, $\beta_0=1$ and pinned-pinned boundary condition.

Table 1
Accuracy of the first dimensionless buckling flow velocity (U_d) of the classical pipe conveying fluid for different boundary conditions, without any surrounding support, blood flow and size effects.

	Boundary conditions		
	Pinned-Pinned	Clamped-Pinned	Clamped-Clamped
Ni et al. [73]	3.1416	4.4934	6.2832
Paidoussis [72]	π	≈ 4.49	2π
Present study	3.1416	4.4939	6.2836

Table 2
Comparison of the first dimensionless critical buckling flow velocity (U_d) for different boundary conditions, multi-phase blood flow, without surrounding support, hematocrit 40% and no size effect theories.

	Boundary conditions		
	Pinned-Pinned	Clamped-Pinned	Clamped-Clamped
Hosseini and Paparisabet [13]	2.7465	3.9282	5.4929
Present study	2.7493	3.9294	5.4982

4.2 Numerical Results

In this section, all calculations are considered for pressure gradient $\frac{dp}{dx} = -67.5 dyne/mm^3$, Young modulus of vessel E=200 *kPa*, plasma density 1025 $kg\ m^{-3}$, RBC density 1125 $kg\ m^{-3}$, plasma viscosity 1.24 *cp*, central core viscosity 2.47 *cp* [3]. Furthermore, another physical parameters such as Poisson ratio, inner and outer radius are considered as v=0.5, 20 μm and 25 μm [75], respectively, and internal material length scales are $l_0 = l_1 = l_2 = l = 17.6\ \mu m$ [66].

Fig. 3 demonstrates the dimensionless eigenvalues versus the dimensionless blood flow velocity based on the MSGT for the various boundary conditions. The parameters hematocrit (40%), structural damping coefficient $g = 0$, compressive pressure $P = 0.1P_{cr}$ and external viscous fluid $C = 0$ are considered. Here P_{cr} *is* critical buckling pressure introduced in [13] as $P_{cr} = \frac{\pi^2 EI}{L^2}$, $P_{cr} = \frac{\pi^2 EI}{(0.7L)^2}$ and $P_{cr} = \frac{\pi^2 EI}{(0.5L)^2}$ for Pinned-Pinned, Clamped-Pinned and Clamped-Clamped boundary conditions, respectively. The results of this section have revealed variation of imaginary and real parts of eigenvalue and critical blood velocity. Imaginary part of eigenvalue, *Im*(Ω), represents the natural frequency of micro blood vessel while real part of eigenvalue, *Re*(Ω), relates to the system decaying rate and indicates it's stability. The positive values of the real part express the unstable oscillations and the negative values means that the system is stable. The blood flow vessel velocity in which the *Im*(Ω)= *Re*(Ω) =0 is known as the critical blood flow velocity and the micro blood vessel loses its stability by buckling. Figs. 3(a) and 3(b), respectively, reveal the imaginary and real parts of the dimensionless eigenvalues of micro blood vessel. In the eigenvalues analysis, it is observed that the micro blood vessel buckles at the first mode and loses stability at the critical blood flow velocity U_d. It is shown by the Fig. 3(a) that due to its higher stiffness, the clamped-clamped boundary condition has a higher dimensionless natural frequency in comparison to other two boundary conditions.

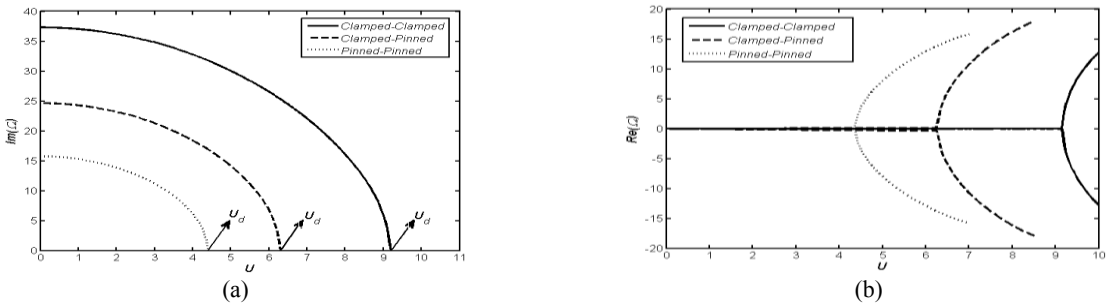

(a) (b)

Fig.3
First non-dimensional eigenvalues of the micro vessel as a function of the blood velocity for *C=0, g=0,* $P=0.1P_{cr}$, hematocrit=40% and different boundary conditions : (a) imaginary parts, (b) real parts.

Fig. 4 displays the dimensionless natural frequency due to the dimensionless internal pressures according to the various theories for $g=0$, $C=0$, U=3 and hematocrit=20% and 40%. This figure shows that the imaginary part of the dimensionless eigenvalues goes higher as the non-classical theories are deployed for pinned-pinned boundary condition. For instance, the MSGT shows higher dimensionless eigenvalues and critical buckling pressure than the MCST. Another interesting fact is that the blood hematocrits have considerable effects on the dimensionless natural frequencies and critical buckling pressures. It is visible from the figure, as the blood hematocrit increases the dimensionless natural frequencies and critical buckling pressures decrease and this phenomenon is regardless of the theories.

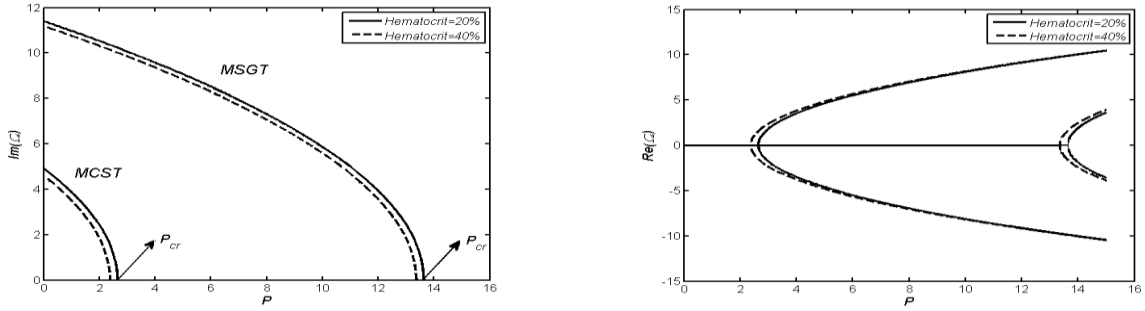

(a) (b)

Fig.4
First non-dimensional eigenvalues of the pinned-pinned micro vessel versus the internal pressure for C=0, g=0, U=3 and different hematocrits: (a) imaginary parts, (b) real parts.

The effect of different radius of vessels on the eigenvalues and critical buckling velocity of a clamped-clamped MBV conveying blood is examined in the Fig. 5 for $C=0$, $g=0$, $P=0.1P_{cr}$, and hematocrit=40%.The critical buckling blood flow velocity and its sensitivity to geometric parameters of a MBV is of great importance. It is observed that the natural frequency and critical buckling velocity decrease with increase in the MBV radius. In other words, by taking constant thickness, the MBV with smaller radius buckle at higher blood flow velocity.

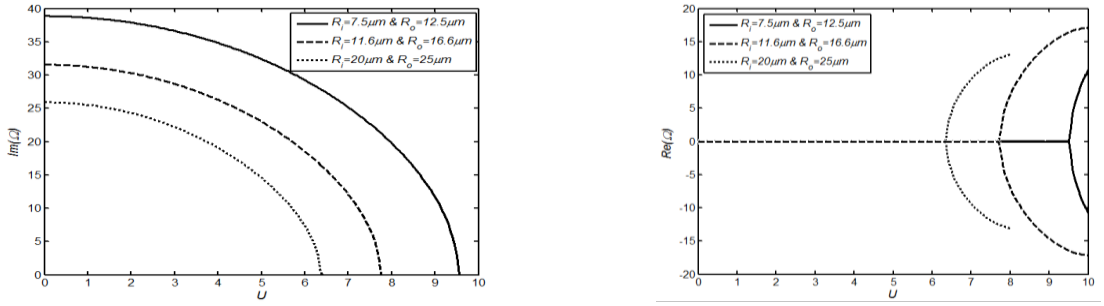

(a) (b)

Fig.5
First non-dimensional eigenvalues of the clamped-clamped micro vessel versus the blood velocity for C=0, g=0, P=0.1P_{cr}, hematocrit=40% and different R_i and R_o: (a) imaginary parts, (b) real parts.

Figs 6 (a) and 6(b) explain the lowest frequencies and decaying rates of clamped-clamped micro blood vessels as a function of the external viscous fluid, respectively, for selected values of $g=0.001$, U=3, $P=0.1P_{cr}$ and different blood hematocrit 20% and 40%. It is revealed that by the increasing of fluid viscosity, the natural frequency decreases, while the decaying rate remain negative, so the amplitude decrements with time and the vibration of the micro blood vessel is damped. Moreover, it is found that by increasing fluid viscosity, the natural frequency becomes zero while the decaying rate is nonzero. This means that the micro blood vessel does not vibrate in the first mode for all theories. It is observed that the large values of hematocrit gives lower eigenvalues. In addition, it can be seen that eigenvalues obtained from the micro blood vessel including the MSGT are higher than those of the MCST and CT.

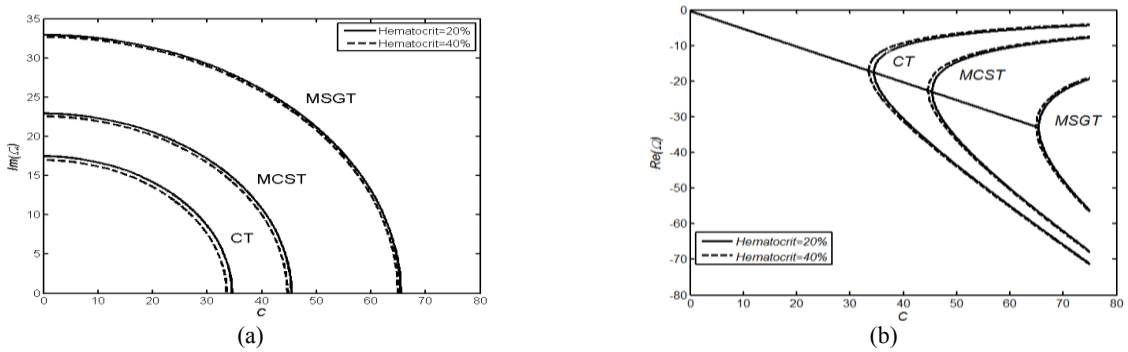

Fig.6
First non-dimensional eigenvalues of the clamped-clamped micro vessel as a function of the viscosity fluid for g=0.001, P=0.1P_{cr}, U=3 and different hematocrits: (a) imaginary parts, (b) real parts.

Fig. 7 explains the relation between the dimensionless critical buckling blood flow velocity and the mass ratio (β_0) for the various theories in clamped-pinned boundary condition when $C=10$, $g=0.001$ and $P=0.1P_{cr}$. The lines in this figure display the buckling boundary. It is found for the small values of mass ratio, the critical flow velocity decreases significantly. Another considerable fact is that the MSGT shows the higher buckling velocities rather than the two other theories.

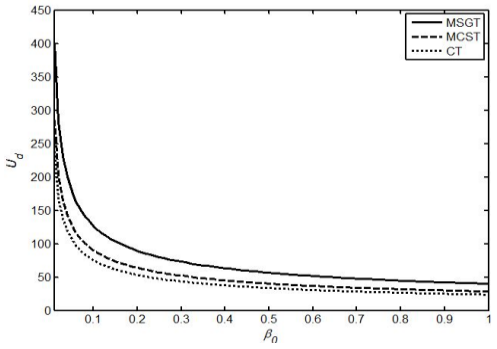

Fig.7
The critical buckling blood flow velocity of the clamped-pinned micro vessel in term of β_0 for C=10, g=0.001, P=0.1P_{cr}.

Fig. 8 demonstrates the relation between the dimensionless critical buckling velocity due to the dimensionless internal pressure for the various hematocrits and boundary conditions. It is shown that the clamped-clamped boundary condition represents the higher dimensionless critical buckling velocities, which is associated with increase of the system stability. It is clear that as the P/P_{cr} is increases, the critical buckling velocity decreases.

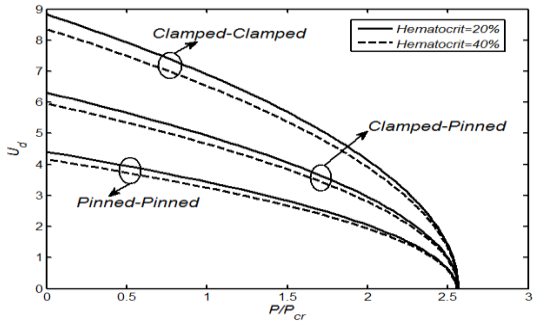

Fig.8
The critical buckling blood flow velocity of the micro vessel in term of the internal pressure for C=10, g=0.001 and different hematocrits based on the MSGT.

To better illustrate the effects of hematocrit on the natural frequency of clamped-clamped MBV, similar calculation is also implemented, and the corresponding result is plotted in Fig. 9 for $P=0.1P_{cr}$, $g=0.001$, $C=10$ and the MSGT. It is revealed that by increasing the value of hematocrit, the natural frequency and critical buckling blood flow velocity of the system decrease. This is due to the fact that by increasing hematocrit in blood,

the modification factors are incremented, and therefore, the centrifugal and Coriolis forces thorough the blood vessel increases and this reasons a decrease in natural frequency and critical blood velocities.

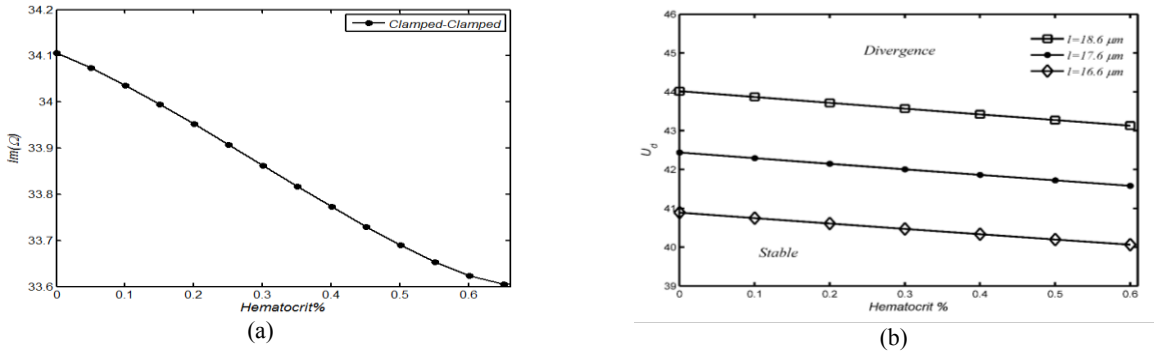

(a) (b)

Fig.9
The effect of the hematocrit on the dimensionless (a) natural frequency for $U=2$ and (b) critical buckling blood velocity of a clamped-clamped MBV, when $P=0.1P_{cr}$, $C=10$, $g=0.001$ and MSGT.

5 CONCLUSION

In this paper, the mechanical behavior of the vessels conveying blood flow resting on viscous fluid based on the MSGT was investigated. The non-uniformity of the various blood flow phases was considered by modification factors. Non-classical beam theories were deployed in order to make much accurate model of the micro blood vessels. Meanwhile, surrounding tissues were modeled by the means of a viscous fluid that embraces the blood vessel. This kind of support model is much more realistic and much more easer to face in the experimental events. Lastly, using the Galerkin method, various numerical results were examined to obtain the effects of length scale parameter, blood flow, internal pressure, structural damping coefficient, viscous fluid substrate and boundary conditions on the mechanical behaviors of system. The results show that the hematocrit has a considerable effect on the natural frequencies, critical blood flow velocities and buckling internal pressure. In addition, it was shown that the MSGT revealed the highest natural frequency, critical blood flow velocity and buckling internal pressure among other theories. Moreover, it is illustrated that the clamped-clamped boundary condition predicts the highest natural frequency in compression to the other boundary conditions. At last, we hope this literature slightly enlighten the future path for the revolutionary surgeries techniques.

REFERENCES

[1] Kakisis J.D., Liapis C.D., Breuer C., Sumpio B.E., 2005, Artificial blood vessel: the holy grail of peripheral vascular surgery, *Journal of vascular surgery* **41**(2): 349-354.
[2] Han H-C., 2008, Nonlinear buckling of blood vessels: a theoretical study, *Journal of Biomechanics* **41**(12): 2708-2713.
[3] Han H-C., 2009, Blood vessel buckling within soft surrounding tissue generates tortuosity, *Journal of Biomechanics* **42**(16): 2797-2801.
[4] Nakamachi E., Uchida T., Kuramae H., Morita Y.,2014, Multiscale finite element analyses for stress and strain evaluations of braid fibril artificial blood vessel and smooth muscle cell, *International Journal for Numerical Methods in Biomedical Engineering* **30**(8): 796-813.
[5] Boileau E., 2015, A benchmark study of numerical schemes for one dimensional arterial blood flow modelling, *International Journal for Numerical Methods in Biomedical Engineering* **31**(10).
[6] Mustapha N., Mandal P.K., Johnston P.R., Amin N., 2010, A numerical simulation of unsteady blood flow through multi-irregular arterial stenosis, *Applied Mathematical Modelling* **34**(6): 1559-1573.
[7] Haghighi A.R., Asl M.S., Kiyasatfar M., 2015, Mathematical modeling of unsteady blood flow through elastic tapered artery with overlapping stenosis, *Journal of the Brazilian Society of Mechanical Sciences and Engineering* **37**(2): 571-578.
[8] Haghighi A.R., Chalak S.A., 2017, Mathematical modeling of blood flow through a stenosed artery under body acceleration, *Journal of the Brazilian Society of Mechanical Sciences and Engineering* **39**(7): 2487-2494.

[9] de Azevedo B.A., Azevedo L.F., Nunes R., Nóbrega A.C., 2015, In vivo blood velocity measurements with particle image velocimetry in echocardiography using spontaneous contrast, *Journal of the Brazilian Society of Mechanical Sciences and Engineering* **37**(2): 559-569.

[10] Han H-C., 2009, The theoretical foundation for artery buckling under internal pressure, *Journal of Biomechanical Engineering* **131**(12): 124501.

[11] Liu Q., Han H-C., 2012, Mechanical buckling of artery under pulsatile pressure, *Journal of Biomechanics* **45**(7): 1192-1198.

[12] Khalafvand S.S., Han H-C., 2015, Stability of carotid artery under steady-state and pulsatile blood flow: A fluid–structure interaction study, *Journal of Biomechanical Engineering* **137** (6): 061007.

[13] Hosseini M., Paparisabet M., 2016, The effects of blood flow on blood vessel buckling embedded in surrounding soft tissues, *International Journal of Applied Mechanics* **8**(5):1650065.

[14] Xiong G., Figueroa C.A., Xiao N., Taylor C.A., 2011, Simulation of blood flow in deformable vessels using subject specific geometry and spatially varying wall properties, *International Journal for Numerical Methods in Biomedical Engineering* **27**(7): 1000-1016.

[15] Sun Q., Wu G.X., 2013, Coupled finite difference and boundary element methods for fluid flow through a vessel with multibranches in tumours, *International Journal for Numerical Methods in Biomedical Engineering* **29**(3): 309-331.

[16] Bouchnita A., Galochkina T., Kurbatova P., Nony P., Volpert V., 2016, Conditions of microvessel occlusion for blood coagulation in flow, *International Journal for Numerical Methods in Biomedical Engineering* **00**:2-27.

[17] Srivastava V., 2007, A theoretical model for blood flow in small vessels, *Applications and Applied Mathematics* **2**(1): 51-65.

[18] McDonald D., 1960, *Blood Flow in Arteries*, Edward Arnold Ltd, London.

[19] Fung Y., 1968, Biomechanics, its scope, history and some problems of continuum mechanics in physiology, *Applied Mechanics Reviews* **21**(1): 1-20.

[20] Hall J.E.,2015, *Guyton and Hall Textbook of Medical Physiology*, Elsevier Health Sciences.

[21] Haynes R.H., Burton A.C., 1959, Role of the non-newtonian behavior of blood in hemodynamics, *American Journal of Physiology-Legacy Content* **197**(5): 943-950.

[22] Hershey D., Byrnes R., Deddens R., Rao A., 1964, *Blood Rheology: Temperature Dependence of the Power Law Model*, AI Ch. E. Boston.

[23] Hosseini M., Fazelzadeh S., 2011, Thermomechanical stability analysis of functionally graded thin-walled cantilever pipe with flowing fluid subjected to axial load, *International Journal of Structural Stability and Dynamics* **11**(03): 513-534.

[24] Eftekhari M., Hosseini M., 2015, On the stability of spinning functionally graded cantilevered pipes subjected to fluid-thermomechanical loading, *International Journal of Structural Stability and Dynamics* **16**(09):1550062.

[25] Lu P., Sheng H., 2012, Exact eigen-relations of clamped-clamped and simply supported pipes conveying fluids, *International Journal of Applied Mechanics* **4**(03): 1250035.

[26] Wang L., Zhong Z., 2015, Radial basis collocation method for the dynamics of rotating flexible tube conveying fluid, *International Journal of Applied Mechanics* **7**(03): 1550045.

[27] Arani A.G., Rastgoo A., Arani A.G., Kolahchi R., 2016, Vibration analysis of carotid arteries conveying non-newtonian blood flow surrounding by tissues, *Journal of Solid Mechanics* **8**(4): 693-704.

[28] Ma Q., Clarke D.R., 1995, Size dependent hardness of silver single crystals, *Journal of Materials Research* **10**(04): 853-863.

[29] Lam D.C., Chong A., 1999, Indentation model and strain gradient plasticity law for glassy polymers, *Journal of Materials Research* **14**(09): 3784-3788.

[30] McFarland A.W., Colton J.S., 2005, Role of material microstructure in plate stiffness with relevance to microcantilever sensors, *Journal of Micromechanics and Microengineering* **15**(5): 1060.

[31] Ziaee S., 2015, Small scale effect on linear vibration of buckled size-dependent FG nanobeams, *Ain Shams Engineering Journal* **6**(2): 587-598.

[32] Eringen A.C., 2002, *Nonlocal Continuum Field Theories*, Springer Science & Business Media.

[33] Yang F., Chong A., Lam D.C.C., Tong P., 2002, Couple stress based strain gradient theory for elasticity, *International Journal of Solids and Structures* **39**(10): 2731-2743.

[34] Lam D.C.C., Yang F., Chong A., Wang J., Tong P., 2003, Experiments and theory in strain gradient elasticity, *Journal of the Mechanics and Physics of Solids* **51**(8): 1477-1508.

[35] Hosseini M., Sadeghi-Goughari M., 2016, Vibration and instability analysis of nanotubes conveying fluid subjected to a longitudinal magnetic field, *Applied Mathematical Modelling* **40**(4): 2560-2576.

[36] Bahaadini R., Hosseini M., 2016, Effects of nonlocal elasticity and slip condition on vibration and stability analysis of viscoelastic cantilever carbon nanotubes conveying fluid, *Computational Materials Science* **114**: 151-159.

[37] Bahaadini R., Hosseini M., 2018, Flow-induced and mechanical stability of cantilever carbon nanotubes subjected to an axial compressive load, *Applied Mathematical Modelling* **59**: 597-613.

[38] Bahaadini R., Hosseini M., 2016, Nonlocal divergence and flutter instability analysis of embedded fluid-conveying carbon nanotube under magnetic field, *Microfluidics and Nanofluidics* **20**(7): 108.

[39] Bahaadini R., Saidi A.R., Hosseini M., 2019, Flow-induced vibration and stability analysis of carbon nanotubes based on the nonlocal strain gradient Timoshenko beam theory, *Journal of Vibration and Control* **25**(1): 203-218.

[40] Bahaadini R., Hosseini M., Jamalpoor A., 2017, Nonlocal and surface effects on the flutter instability of cantilevered nanotubes conveying fluid subjected to follower forces, *Physica B: Condensed Matter* **509**: 55-61.
[41] Bahaadini R., Hosseini M., Jamali B., 2018, Flutter and divergence instability of supported piezoelectric nanotubes conveying fluid, *Physica B: Condensed Matter* **529**: 57-65.
[42] Bahaadini R., Saidi A.R., Hosseini M., 2018, Dynamic stability of fluid-conveying thin-walled rotating pipes reinforced with functionally graded carbon nanotubes, *Acta Mechanica* **229**(12): 5013-5029.
[43] Bahaadini R., Hosseini M., Khalili-Parizi Z., 2019, Electromechanical stability analysis of smart double-nanobeam systems, *The European Physical Journal* **134**(7): 320.
[44] Bahaadini R., Dashtbayazi M.R., Hosseini M., Khalili-Parizi Z., 2018, Stability analysis of composite thin-walled pipes conveying fluid, *Ocean Engineering* **160**: 311-323.
[45] Bahaadini R., Saidi A.R., Arabjamaloei Z., Ghanbari-Nejad-Parizi A., 2019, Vibration analysis of functionally graded graphene reinforced porous nanocomposite shells, *International Journal of Applied Mechanics* **11**(7): 1950068.
[46] Bahaadini R., Saidi A.R., 2019, Aerothermoelastic flutter analysis of pre-twisted thin-walled rotating blades reinforced with functionally graded carbon nanotubes, *European Journal of Mechanics-A/Solids* **75**: 285-306.
[47] Bahaadini R., Saidi A.R., 2018, On the stability of spinning thin-walled porous beams, *Thin-Walled Structures* **132**: 604-615.
[48] Bahaadini R., Saidi A.R., 2018, Aeroelastic analysis of functionally graded rotating blades reinforced with graphene nanoplatelets in supersonic flow, *Aerospace Science and Technology* **80**: 381-391.
[49] Bahaadini R., Saidi A.R., 2018, Stability analysis of thin-walled spinning reinforced pipes conveying fluid in thermal environment, *European Journal of Mechanics-A/Solids* **72**: 298-309.
[50] Saidi A.R., Bahaadini R., Majidi-Mozafari K., 2019, On vibration and stability analysis of porous plates reinforced by graphene platelets under aerodynamical loading, *Composites Part B: Engineering* **164**: 778-799.
[51] Mohammadi K., Barouti M.M., Safarpour H., Ghadiri M., Effect of distributed axial loading on dynamic stability and buckling analysis of a viscoelastic DWCNT conveying viscous fluid flow, *Journal of the Brazilian Society of Mechanical Sciences and Engineering* **41**(2): 93.
[52] Cabrera-Miranda J.M., Paik J.K., 2019, Two-phase flow induced vibrations in a marine riser conveying a fluid with rectangular pulse train mass, *Ocean Engineering* **174**: 71-83.
[53] Farajpour A., Farokhi H., Ghayesh M.H., 2019, Chaotic motion analysis of fluid-conveying viscoelastic nanotubes, *European Journal of Mechanics-A/Solids* **74**: 281-296.
[54] Amiri A., Vesal R., Talebitooti R., Flexoelectric and surface effects on size-dependent flow-induced vibration and instability analysis of fluid-conveying nanotubes based on flexoelectricity beam model, *International Journal of Mechanical Sciences* **156**: 474-485.
[55] Ebrahimi F., Hajilak Z.E., Habibi M., Safarpour H., 2019, Buckling and vibration characteristics of a carbon nanotube-reinforced spinning cantilever cylindrical 3D shell conveying viscous fluid flow and carrying spring-mass systems under various temperature distributions, *Proceedings of the Institution of Mechanical Engineers, Part C: Journal of Mechanical Engineering Science* **233**: 4590-4605.
[56] Mohammadimehr M., Mehrabi M., 2017, Stability and free vibration analyses of double-bonded micro composite sandwich cylindrical shells conveying fluid flow, *Applied Mathematical Modelling* **47**: 685-709.
[57] Arani A.G., Shajari A., Atabakhshian V., Amir S., Loghman A., 2013, Nonlinear dynamical response of embedded fluid-conveyed micro-tube reinforced by BNNTs, *Composites Part B: Engineering* **44**(1): 424-432.
[58] Arani A.T., Ghorbanpour Arani A., Kolahchi R., 2015, Non-newtonian pulsating blood flow-induced dynamic instability of visco-carotid artery within soft surrounding visco-tissue using differential cubature method, *Proceedings of the Institution of Mechanical Engineers, Part C: Journal of Mechanical Engineering Science* **229**(16): 3002-3012.
[59] Atashafrooz M., Bahaadini R., Sheibani H.R., 2018, Nonlocal, strain gradient and surface effects on vibration and instability of nanotubes conveying nanoflow, *Mechanics of Advanced Materials and Structures* **27***:* 1-13.
[60] Hosseini M., Maryam A.Z.B., Bahaadini R., 2017, Forced vibrations of fluid-conveyed double piezoelectric functionally graded micropipes subjected to moving load, *Microfluidics and Nanofluidics* **21**(8): 134.
[61] Hosseini M., Bahaadini R., Makkiabadi M., 2018, Application of the Green function method to flow-thermoelastic forced vibration analysis of viscoelastic carbon nanotubes, *Microfluidics and Nanofluidics* **22**(1): 6.
[62] Hosseini M., Bahaadini R., Khalili-Parizi Z., 2019, Structural instability of non-conservative functionally graded micro-beams tunable with piezoelectric layers, *Journal of Intelligent Material Systems and Structures* **30**(4): 593-605.
[63] Soleymani T., Arani A.G., 2019, On aeroelastic stability of a piezo-MRE sandwich plate in supersonic airflow, *Composite Structures* **230**: 111532.
[64] Arani A.G., Soleymani T., 2019, Size-dependent vibration analysis of a rotating MR sandwich beam with varying cross section in supersonic airflow, *International Journal of Mechanical Sciences* **151**: 288-299.
[65] Arani A.G., Soleymani T., 2019, Size-dependent vibration analysis of an axially moving sandwich beam with MR core and axially FGM faces layers in yawed supersonic airflow, *European Journal of Mechanics-A/Solids* **77**: 103792.
[66] Yin L., Qian Q., Wang L., 2011, Strain gradient beam model for dynamics of microscale pipes conveying fluid, *Applied Mathematical Modelling* **35**(6): 2864-2873.
[67] Ghavanloo E., Fazelzadeh S.A., 2011, Flow-thermoelastic vibration and instability analysis of viscoelastic carbon nanotubes embedded in viscous fluid, *Physica E: Low-dimensional Systems and Nanostructures* **44**(1): 17-24.

[68] Haynes R.H., 1960, Physical basis of the dependence of blood viscosity on tube radius, *American Journal of Physiology-Legacy Content* **198**(6): 1193-1200.
[69] Benjamin T.B., 1961, Dynamics of a System of articulated pipes conveying fluid. I. Theory, *Proceedings of the Royal Society of London, Series A, Mathematical and Physical Sciences* **261**(1307): 457-486.
[70] Bahaadini R., Hosseini M., 2016, Nonlocal divergence and flutter instability analysis of embedded fluid-conveying carbon nanotube under magnetic field, *Microfluidics and Nanofluidics* **20**(7): 1-14.
[71] Hosseini M., Bahaadini R., Jamali B., 2016, Nonlocal instability of cantilever piezoelectric carbon nanotubes by considering surface effects subjected to axial flow, *Journal of Vibration and Control* **24**:1908-1825.
[72] Paidoussis M.P., *1998, Fluid-Structure Interactions: Slender Structures and Axial Flow*, Academic Press.
[73] Ni Q., Zhang Z.L., Wang L., 2011, Application of the differential transformation method to vibration analysis of pipes conveying fluid, *Applied Mathematics and Computation* **217**(16): 7028-7038.
[74] Guo C., Zhang C., Païdoussis M., 2010, Modification of equation of motion of fluid-conveying pipe for laminar and turbulent flow profiles, *Journal of Fluids and Structures* **26**(5): 793-803.
[75] Qin S., Ferrara K.W., 2007, The natural frequency of nonlinear oscillation of ultrasound contrast agents in microvessels, *Ultrasound in Medicine & Biology* **33**(7): 1140-1148.